J Mater Sci (2018) 53:7083–7093

Polymers

Improving the crystallization and fire resistance of poly(lactic acid) with nano-ZIF-8@GO

Mi Zhang[1], Xiaowei Shi[1], Xiu Dai[1], Changan Huo[1], Jiong Xie[1], Xu Li[1], and Xinlong Wang[1,*]

[1] School of Chemical Engineering, Nanjing University of Science and Technology, Nanjing 210094, China

Received: 9 November 2017
Accepted: 16 January 2018
Published online: 24 January 2018

ABSTRACT

The nano-ZIF-8@GO hybrids were synthesized and blended with poly(lactic acid) (PLA) by solution method. The effect of nano-ZIF-8@GO hybrids on the crystallization was investigated by DSC and POM. The results showed that low addition amount of nano-ZIF-8@GO had a significant influence on the crystallization behavior of PLA. The tensile strength and elongation at break of the PLA/ZIF-8@GO nanocomposites with 0.5 wt% of ZIF-8@GO were increased to 49.63 MPa and 24.10% compared with 35.83 MPa and 17.66% of the pure PLA, respectively. The addition of nano-ZIF-8@GO hybrids also enhanced the flame retardancy of PLA, and the mechanism was proposed.

Introduction

Poly(lactic acid) (PLA), the best-known degradable polyester from renewable sources such as corn starch, potato starch and sugar beets, is expected to replace the petroleum-based commodity polymers [1]. Although PLA is a very promising polymer in the field of eco-friendly materials, it suffers from slow crystallization rate and easy flammability, which restricts its applications as engineering materials in electronic and automotive industry [2, 3]. The addition of micro- and/or nano-fillers into PLA matrix is considered as a powerful method to improve its properties and obtain specific end-use characteristics [4, 5].

As a two-dimensional carbon material with large surface area and rich functional groups, graphene (oxide) has been used to enhance crystallization rate, mechanical properties, gas barrier, electrical conductivity, flame retardancy of polymers [6–8]. Xu [9] studied the isothermal crystallization of PLA induced by graphene, and the results showed that two-dimensional graphene sheets could serve as nucleating agents in accelerating the crystallization kinetics of PLA. Kim [10] prepared the polymer nanocomposites of graphene oxide sheets with surface porosity and the prepared nanocomposites exhibited significantly improved Young's modulus and tensile strength. The Co_3O_4 functionalized graphene has been prepared to reduce the fire hazards of PLA recently, and it proved that the incorporation of Co_3O_4/graphene into PLA slowed down the heat release rate, which was reduced by 40% compared with that of pure PLA [11, 12]. MOFs are porous polymeric materials consisting of metal ions or clusters linked together by organic bridging ligands [13]. Compared with traditional particles, nano-MOFs particles are well crystalline crystals with high

Address correspondence to E-mail: wxinlong323@163.com

https://doi.org/10.1007/s10853-018-2049-2

specific surface and cavity. Moreover, nano-MOFs have a better affinity with polymer chains since the organic linkers in MOFs can provide strong interactions with polymer chains [14]. The wide-ranged crystallinity, cavity and high specific surface of MOFs are beneficial to the improvement of polymer crystallization and other properties. Merely Elangovan [15] mixed PLA with MOFs known as HKUST-1, and the results showed an increase of 15% in Izod impact strength and 170% in elongation at break.

The MOF@GO hybrids combine the unique advantages of MOF and GO and have been the focus of recent researches [14, 16]. The MOFs nanoparticles anchored on GO sheets inhibit GO sheets to stack together and make them disperse effectively in polymer matrix. Furthermore, the presence of GO sheets restricts agglomeration and improves the stability of nano-MOFs scattered on the surface. A number of hybrids such as ZIF-67@GO, MOF-5@GO, HKUST-1@GO have been reported by Bandosz group [17, 18]. Most of the reported MOFs@GO hybrids have been used in adsorption or catalysis, etc. [17], and few studies have been made about their composites with polymers.

Herein, we prepared nano-ZIF-8@GO hybrids and incorporated them into PLA matrix to fabricate the PLA nanocomposites. Nano-ZIF-8 consists of Zn–O–Zn and imidazole units containing a lot of nitrogen [19]. It is well known that the compounds containing nitrogen or Zn can be applied as flame retardants or synergistic flame retardants. GO has been used to improve the properties of polymers. Inspired by this, we used ZIF-8@GO hybrids to overcome the shortcomings of PLA, especially the slow crystallization rate, low mechanical properties and flammability. The related mechanisms were also discussed.

Experimental

Materials

Poly(lactic acid) (PLA 290) was purchased from Zhejiang Haizheng Biological Materials Co., Ltd, China. 2-Methyl imidazole (98%) was obtained from Shanghai Aladdin Industrial Corporation, China. $Zn(NO_3)_2{\cdot}6H_2O$ was supplied by Xilong Chemical Co., Ltd, China. Methanol (CH_3OH), potassium persulfate ($K_2S_2O_5$), phosphorus pentoxide (P_2O_5) and hydrogen peroxide (H_2O_2) were provided by Sinopharm Chemical Reagent Co., Ltd, China. Chloroform ($CHCl_3$, 99%), concentrated sulfuric acid (H_2SO_4, 95–98%), potassium permanganate ($KMnO_4$) and hydrochloric acid (HCl) were received from Shanghai Lingfeng Chemical Reagent Co., Ltd, China. Natural graphite powders (1–44 μm) were purchased from Sinopharm Chemical Reagent Co., Ltd, China. Deionized water was produced in our lab.

Preparation of the ZIF-8@GO hybrids

An improved Hummers method was used to prepare graphite oxide (GO) [20, 21]. 1.602 g 2-Methyl imidazole and 1.487 g $Zn(NO_3)_2{\cdot}6H_2O$ were dissolved in 100 mL methanol. 0.163 g GO was dispersed in methanol (100 mL) and then added to the above solution with magnetic stirring. The mixture was stirred for 1 h at room temperature. Finally, the ZIF-8@GO hybrids were centrifuged, washed with CH_3OH and dried at 80 °C for 48 h.

Preparation of the PLA/ZIF-8@GO nanocomposites

The dried PLA was dissolved in 40 mL chloroform with magnetic stirring for 2 h. A certain amount of ZIF-8@GO was dispersed in chloroform by sonication to form a homogeneous dispersion and then poured into the PLA solution. The mixture was stirred for 4 h and kept for 30 min to leave the bubbles in the solution. The mixed solution was then cast into a film using an automatic coater (MRXTMH250, Shenzhen Mingruixiang Automation Equipment Co., Ltd.). After the chloroform solvent was evaporated at room temperature, the film was dried in an oven at 50 °C for 48 h to further remove the residual solvent. The PLA nanocomposites with 0, 0.05, 0.5 and 2 wt% ZIF-8@GO were prepared and abbreviated as PLA-0, PLA-1, PLA-2 and PLA-3, respectively. The PLA composite with 0.5 wt% ZIF-8 was also prepared and abbreviated as PLA/ZIF-8.

Measurement and characterization

Morphologies of ZIF-8@GO, ZIF-8 and GO were observed using a JEM-2100 transmission electron microscope (TEM, JEOL JEM-2100, Japan).

X-ray diffraction (XRD) measurements were carried out by Bruker D8 Advance diffractometer

(Germany) at 40 kV and 40 mA with Cu K_α radiation (0.15418 nm). The nanoparticle sizes of both ZIF-8 alone and ZIF-8 on GO sheets were calculated by Scherrer formula [22] as shown below:

$$D = 0.89\lambda/\beta\cos\theta$$

where D is the nanoparticle size, λ is the X-ray wavelength ($\lambda = 0.15418$ nm), β is the full width at half maximum (FWHM) in radiance, and θ is the Bragg angle of diffraction line.

Scanning electron microscope (SEM, Hitachi S-4800, Japan) with an energy dispersive spectrometer (EDS) was employed to observe char residue and fracture morphologies of the PLA nanocomposites.

Differential scanning calorimetry (DSC) measurements were carried out by a Q80 DSC apparatus (TA Corporation, America). Before all DSC tests, the thermal history was removed by heating the samples to 190 °C and maintaining at 190 °C for 5 min. The non-isothermal test was carried out by cooling the samples from 190 °C down to 35 °C by cooling rates of 2 °C/min and then re-heating from 35 °C to 190 °C at a heating rate of 20 °C/min in N_2 atmosphere. The crystallinity (X_c) is determined from the formula as follows:

$$X_c = \Delta H_c/\Delta Ho\, m(1-\varphi)$$

where ΔH_c is the crystallization enthalpy (J/g), $\Delta Ho\, m$ is the melting enthalpy of the 100% crystallized PLA (93.6 J/g) [23], and φ is the mass fraction of the ZIF-8@GO in PLA composites [24].

A polarizing microscope (POM, Jiangnan BM2100PO, China) was used to observe crystal images of the isothermal crystallization. The samples were heated from room temperature to 190 °C and held 5 min to remove the thermal history. Then, the samples were rapidly cooled to 130 °C and then maintained at 130 °C for 8 min.

Tensile testing measurement was measured by ASTM D638 on a CMT tensile tester (Sans, China) at the rate of 10 mm/min at room temperature according to ASTM D638. The values were averaged over five measurements.

Limiting oxygen index (LOI) test was measured five times according to ASTM Standard D2863-97.

Vertical burning (UL-94) test was performed according to ASTM D3801 using a vertical burning tester (CZF-3, Jiangning Analytical Instrument Co., China). The values were averaged over five measurements.

Fourier transform infrared spectroscopy (FTIR) spectra were recorded on FTIR-8400S spectrometer (Shimadzu, Japan) at a range of 400–4000 cm^{-1} with a resolution of 4 cm^{-1}.

Raman spectra was tested on a Renishaw Invia laser Raman spectrometer (England) with the wavenumber range from 500 to 3000 cm^{-1} by using He laser beam excitation.

Results and discussion

Characterization of ZIF-8@GO

Figure 1a shows the TEM image of GO, and it can be seen that the GO sheets present a crumpled surface and are overlapped in a few layers. Figure 1b shows TEM of nano-ZIF-8@GO, and a large amount of uniform ZIF-8 nanoparticles have grown evenly on the surface of the GO sheets, where the red arrows indicate the GO edge. It demonstrates that GO sheets provide platforms for the nucleation and growth of nano-ZIF-8 crystals, and prohibit the agglomeration of ZIF-8 nanoparticles, which may be attributed to the strong interactions between nano-ZIF-8 and GO sheets [25]. The particle size of the ZIF-8 on GO sheets is about 32–45 nm compared with 62–76 nm of that without GO sheets as shown in Fig. 1c. Figure 1d shows the FTIR spectra of GO, ZIF-8 and ZIF-8@GO. The peaks at 1720 and at 1616 cm^{-1} are assigned to the stretching vibrations of C=O and C=C in GO. The peaks at 1588 cm^{-1} and at 1422 cm^{-1} are attributed to the stretching vibrations of C=N and the imidazole ring of ZIF-8. These four characteristic peaks appear in the FTIR of ZIF-8@GO. The TEM and FTIR results confirm the formation of the ZIF-8@GO hybrid material [26].

Figure 2a shows the X-ray diffraction (XRD) patterns of GO, ZIF-8 and ZIF-8@GO. There is a strong peak at $2\theta = 10.85°$ in GO pattern, which corresponds to (002) reflections of GO [27]. The characteristic peaks of ZIF-8 marked in the figure are consistent with the literature as reported [28]. The peaks between 5° and 40° of ZIF-8 could be found in the pattern of ZIF-8@GO, but the (002) reflection of GO is absent, which may be ascribed to the damage of the regular stack of GO [29, 30]. The XRD analysis indicates the formation of ZIF-8@GO further. Moreover, the nanoparticle sizes of both ZIF-8 alone and ZIF-8 on GO sheets were calculated and are shown in

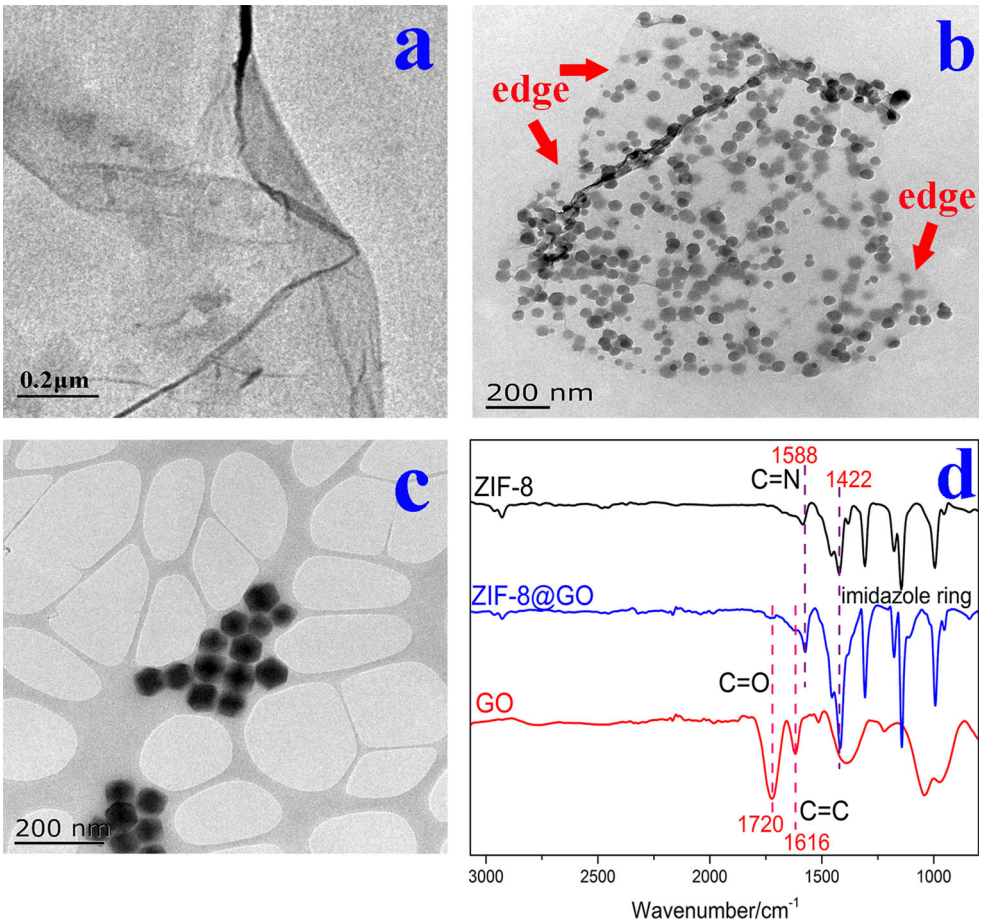

Figure 1 TEM of GO (**a**), nano-ZIF-8@GO (**b**), ZIF-8 (**c**) and the FTIR spectra of GO, ZIF-8 and ZIF-8@GO (**d**).

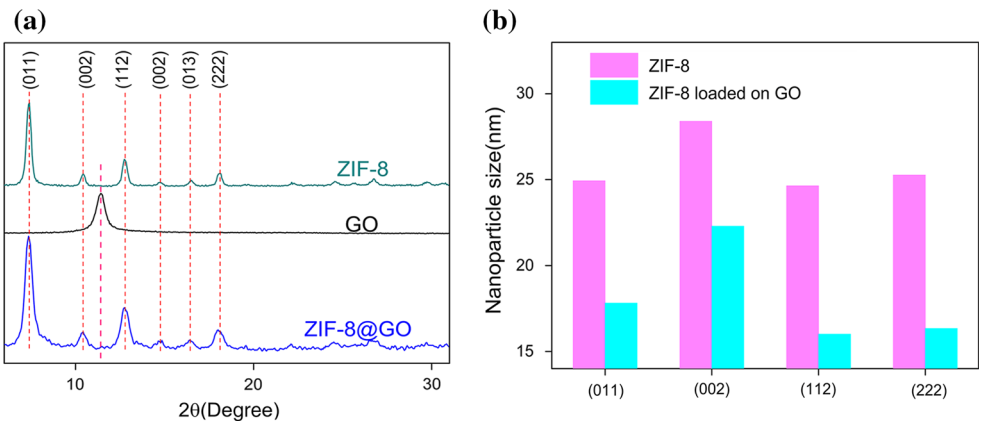

Figure 2 XRD of GO, ZIF-8 and ZIF-8@GO (**a**) and the nanoparticle size of ZIF-8 (**b**).

Fig. 2b. It can be seen that the ZIF-8 particles loaded on GO sheets are smaller than those unloaded as shown in Fig. 1c. It may be attributed to that the ZIF-8 sizes are probably controlled by –OH and –COOH groups of GO through coordination modulation which inhibits the growth of large crystals [25].

FTIR of the PLA nanocomposites

The formation of the PLA nanocomposites is confirmed by digital photos and FTIR as shown in Fig. 3. The photos show that the nanocomposites are light brown with good transparency. It can be seen that all the characteristic peaks of the composites are in agreement with pure PLA in Fig. 3b, c, which

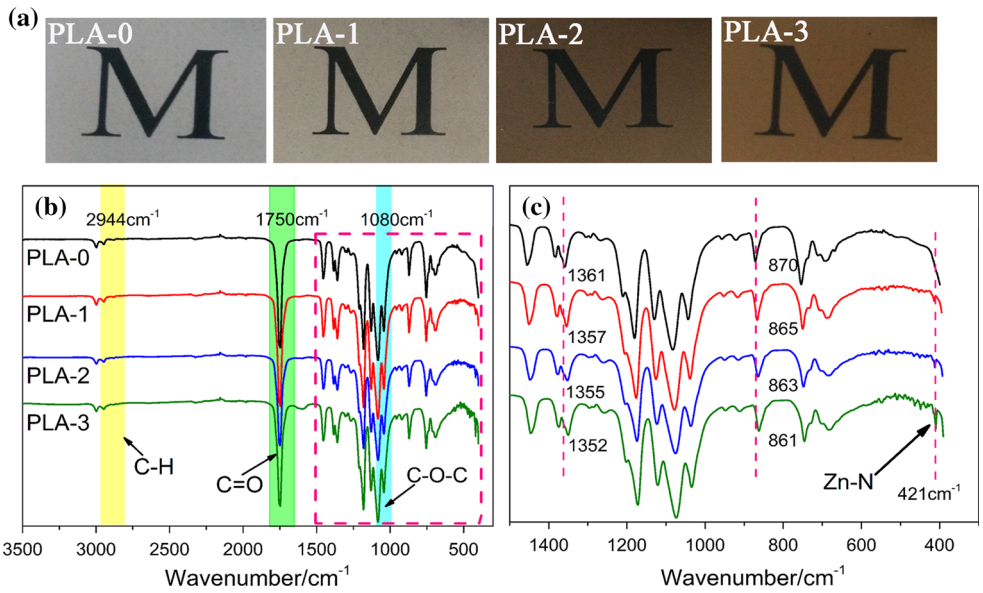

Figure 3 Digital photos (**a**) and FTIR spectra (**b**) of the PLA composites.

confirms the incorporation of ZIF-8@GO does not affect the molecular structure of PLA. The peak at 2944 cm^{-1} is attributed to the asymmetric stretching vibration of C-H. The peaks at 1750 and 1080 cm^{-1} are corresponded to the stretching vibration of C=O and C–O–C, respectively [31]. It is noteworthy that the peaks at ca. 1361–870 cm^{-1} are slightly shifted toward lower wavenumber, which could be due to the strong interaction between PLA and ZIF-8@GO. There is an additional characteristics peak at 421 cm^{-1} in the nanocomposites which is assigned to Zn-N, indicating the presence of ZIF-8@GO in the composites [26]. However, the characteristic peaks of GO are overlapped with that of PLA.

SEM of the PLA nanocomposites

The fractured surface morphology of pure PLA is shown in Fig. 4a, which shows a smooth and clean surface. The image of PLA-2 with 0.5 wt% ZIF-8@GO is shown in Fig. 4b, and the EDS in Fig. 4c proves the presence of ZIF-8@GO in the nanocomposites further. From Fig. 4b, it can be seen that the ZIF-8@GO particles are well-dispersed in the nanocomposites and no large agglomerates are observed, which indicates that the ZIF-8@GO particles have excellent interface compatibility with PLA [32]. The strong interactions between the organic linkers in ZIF-8 and PLA chains provide good affinity for ZIF-8@GO with PLA. Moreover, the ZIF-8 nanoparticles anchored on the GO sheets prevent GO from stacking together and make them to disperse well in the PLA matrix.

Non-isothermal DSC of the PLA nanocomposites

The non-isothermal DSC tests were carried out at a cooling rate of 2 °C/min. Figure 5a, b presents the cooling and subsequent re-heating traces of the PLA nanocomposites, respectively. We can get some information such as glass transition, melting and crystallization from the curves. The PLA nanocomposites show slightly higher glass transition temperatures (T_g) than that of pure PLA. The increase of T_g may be explained that the presence of ZIF-8@GO crystals destroys the integrity of the PLA structure, impeding the movement of the PLA chains [33]. The crystallization temperature (T_c) of pure PLA is about 122 °C. By contrast, the T_cs of PLA nanocomposites are higher as the ZIF-8@GO concentration increased, which shows that PLA nanocomposites start to crystallize earlier than pure PLA under non-isothermal conditions, manifesting the nucleating effect of ZIF-8@GO on the crystallization of PLA. The presence of ZIF-8@GO particles in the PLA matrix can locally multiply the number of crystal nucleus, and it will be easier for the PLA chains to reach one nucleus, reducing the displacement and enhancing the local mobility [34]. From Fig. 5b, it can be seen that the melting temperature (T_m) of the PLA nanocomposites is also decreased and double melting peaks appear for all samples. The reduction in T_m may be due to the lower perfect crystal brought about by the fast crystallization rate [35]. The appearance of double

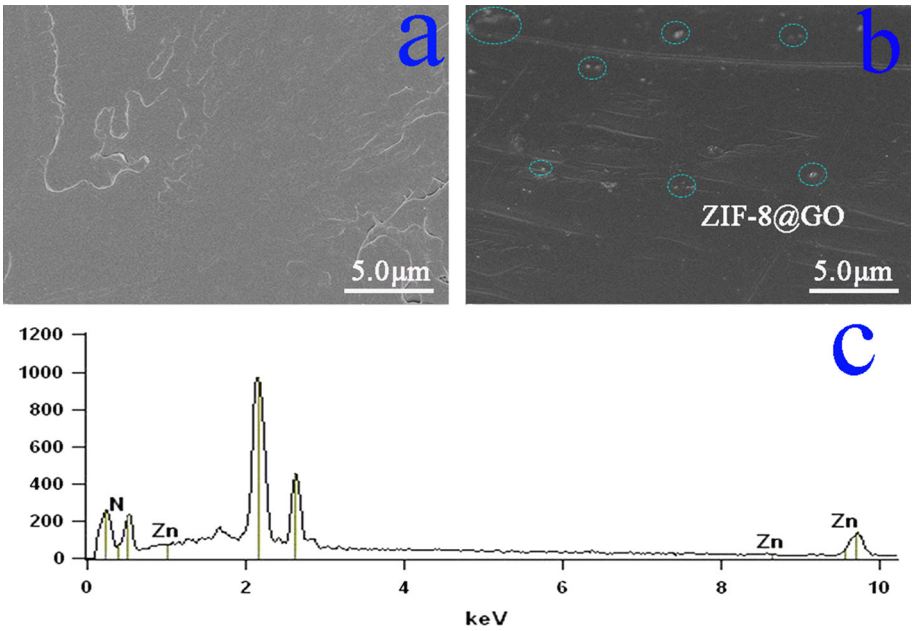

Figure 4 SEM of PLA-0 (**a**), PLA-2 (**b**) and EDS (**c**) of PLA-2.

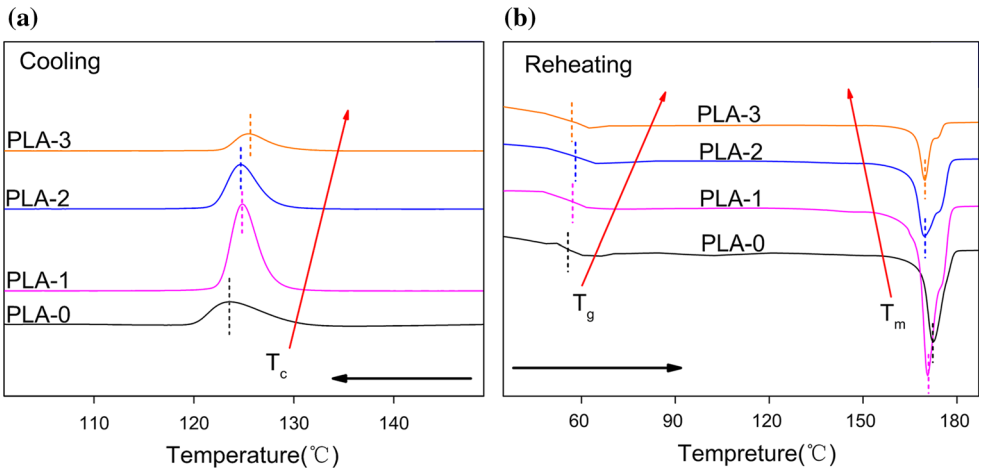

Figure 5 DSC of the nanocomposites at cooling rates of 2 °C/min.

melting peak is attributed to the presence of different crystal forms and re-melting process [36].

The crystallinities of the nanocomposites are shown in Fig. 6a. The crystallinity of PLA-1 is increased to about 69.5% in comparison with 36.3% of

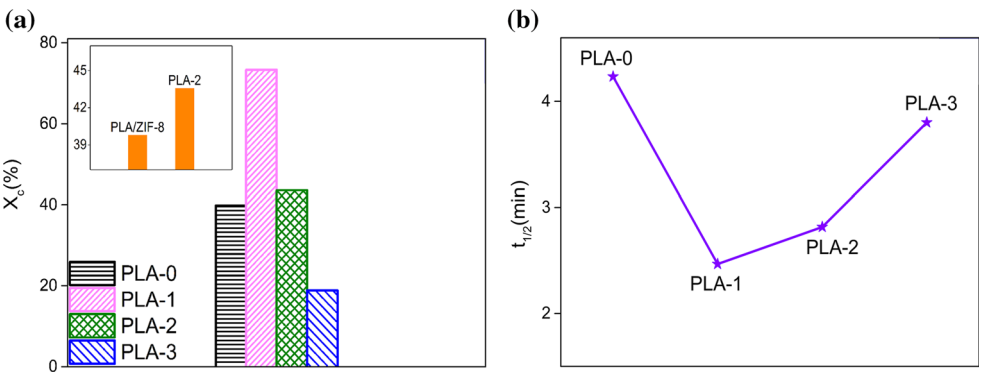

Figure 6 The crystallinity X_c (**a**) and $t_{1/2}$ (**b**) of the nanocomposites.

pure PLA at 2 °C/min cooling rate, which indicates that the ZIF-8@GO particles may play a nucleating role in crystallization of PLA. However, the crystallinity of PLA-3 is decreased owing to the agglomeration of the large amount of ZIF-8@GO existing in the PLA matrix. The crystallization rate can be judged by the semicrystallization time $t_{1/2}$, and the $t_{1/2}$ of the nanocomposites is shown in Fig. 6b. Figure 6b shows that the $t_{1/2}$ presents a "*u*" shape and $t_{1/2}$ decreases as the addition of ZIF-8@GO. We could associate the crystallization rate to two collaborative processes: the crystal growth rate and the production rate of nuclei [37]. When adding ZIF-8@GO particles in PLA matrix, on the one hand, the PLA nanocomposites will mostly experience heterogeneous nucleation induced by ZIF-8@GO particles. On the other hand, the ZIF-8@GO particles may have an enhanced effect on both the crystal growth rate and the production rate of nuclei, resulting in the increase in the crystallization rate.

POM of the nanocomposites

Figure 7 presents the polarizing microscope (POM) crystal images of the PLA nanocomposites. With reference to the semicrystallization time exhibited in Fig. 6b, we adopt 8 min (about double semicrystallization time) as the isothermal crystallization time. After isothermal crystallization for 8 min, the emergence of crystals for pure PLA and the nanocomposites can be observed. The crystal gradually grows perfect, and the spherulites with a relatively complete morphology can be seen. The phenomenon reveals that the presence of ZIF-8@GO nanoparticles does not change the three-dimensional growth of PLA crystals [23]. Meanwhile, it is evident that the number of the crystals in the PLA-1 is more than that of pure PLA. However, the crystal density of PLA-3 is decreased compared with pure PLA.

As shown in DSC and POM, the addition of ZIF-8@GO affects the crystallization of PLA obviously. The ZIF-8@GO nanoparticles in a good dispersion in PLA matrix act as crystallization centers. Not only the nano-ZIF-8 with high porosity, well crystalline property and high specific surface influences the crystallization behavior, the presence of GO with high specific surface and the interactions between PLA molecules and ZIF-8@GO also promote the crystallization [38–40]. This can be proved from the comparison with the sample containing nano-ZIF-8 alone. The crystallinity and $t_{1/2}$ of the sample PLA/ZIF-8 with 0.5 wt% ZIF-8 are calculated from its DSC at cooling rates of 2 °C/min and exhibited in Fig. 6. The crystallinity and the $t_{1/2}$ of PLA/ZIF-8 are 39.8% and 3.5 min, while the values for PLA-2 are 43.6% and 2.8 min, respectively. About the crystallization mechanism, during the crystallization process the ZIF-8@GO crystals first absorb the PLA chains to the surface of ZIF-8@GO to increase crystalline regions and limit the movement of PLA chains, and then the absorbed PLA chains start to orient [41], which induces the crystallization.

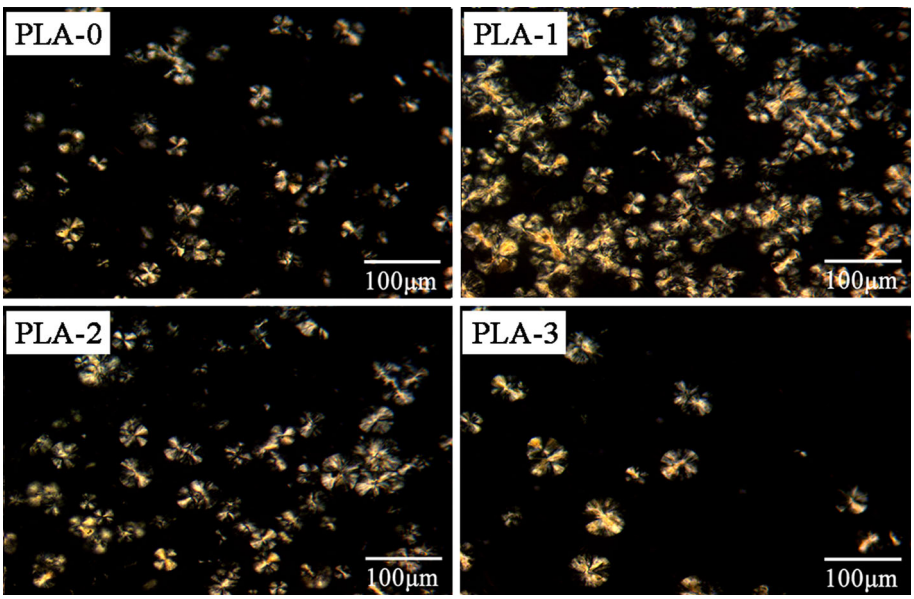

Figure 7 The isothermal crystallization POM of the nanocomposites at 130 °C for 8 min.

Mechanical properties of the PLA nanocomposites

The mechanical properties of the PLA nanocomposites are tested, and the results are presented in Fig. 8. The tensile strength of pure PLA is around 35.83 MPa with 17.66% elongation at break, which is coincided with the fact that PLA is a rigid polymer [42]. The addition of ZIF-8@GO induces a growing trend for tensile strength. For example, the PLA-2, with the content of 0.5 wt% ZIF-8@GO, exhibits the tensile strength of 49.63 MPa and 24.1% elongation at break, respectively. The enhancement of mechanical properties can be explained by the well-dispersion of ZIF-8@GO crystals in PLA matrix. Apart from this, the high aspect ratio of nano-ZIF-8 and GO can entrap large number of PLA chains on their surfaces, which leads to the strong filler/matrix interactions and good reinforcement effects [43]. In the case of elongation at break, the interparticle distance also makes some contribution to the increase [44]. The role of GO on the reinforcement can be explained by comparing the tensile strength of PLA/ZIF-8 with that of PLA-2 in Fig. 8. The tensile strength of PLA/ZIF-8 is 42.92 MPa which is lower than that of PLA-2. With the loading of ZIF-8@GO to 2 wt%, the values of tensile strength and elongation have an abrupt reduction, which is due to the filler agglomeration that causes the formation of cracks and the decrease in mechanical properties [45].

Flame retardancy and mechanism consideration of the PLA nanocomposites

The flammability properties of the PLA nanocomposites were analyzed by LOI and UL-94 vertical burning test, and the results are summarized in

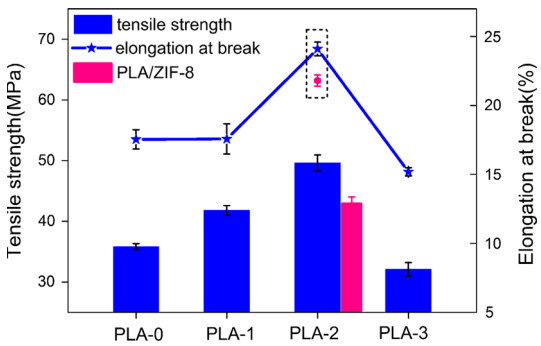

Figure 8 The tensile strength and elongation at break of the PLA nanocomposites.

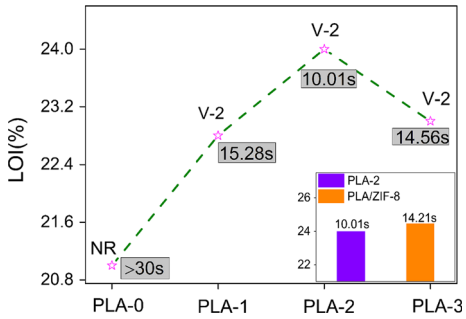

Figure 9 LOI and UL-94 results of the nanocomposites.

Fig. 9. It is generally believed that pure PLA is a flammable polymer with a LOI value of 21.0% and not classified in the UL-94 rating [46]. For the PLA nanocomposites, the LOI increases and reaches the maximum when the ZIF-8@GO content is 0.5 wt%. Meanwhile, the self-extinguishing time in UL-94 vertical burning test is getting shorter and shorter, and the UL-94 test of the nanocomposites reaches V-2 rating. These show that ZIF-8@GO can play as an effective flame retardant for PLA. There is a slight reduction in both LOI and self-extinguishing time for PLA-3 due to the agglomeration of ZIF-8@GO.

In order to study the effect of ZIF-8@GO on the flame retardancy of PLA further, we investigate its residual char in detail with PLA-2 as a typical representative. Figure 10a shows the SEM image of the char residue, and a continuous dense char layer is observed. The FTIR of the char residue is shown in Fig. 10b. The peaks at around 3852 and 3783 cm^{-1} are attributed to O–H or N–H. The peak at 1702 cm^{-1} is attributed to the C=O bonding stretching vibration. The peaks at 1640 and 1520 cm^{-1} are corresponded to the stretching modes of the residual aromatic ring structure. In addition, the char residues also show absorptions at approximately 506 and 433 cm^{-1} ascribed to the asymmetric stretching vibration of ZnO. Figure 10c shows the XRD pattern of the char residue. There is a strong and broad peak at $2\theta = 26.38°$ which belongs to (002) of graphite. Figure 10d presents the Raman spectra, and it can be observed that the curve presents two peaks at 1340 and 1575 cm^{-1} corresponding to D and G band, respectively. The D band is attributed to the disorder graphitic structure, while the G band is assigned to oriented graphitic structure [47]. The curves of Raman and XRD manifest no perfect graphite in the char residue of PLA-2 nanocomposites, which means that the char residue is only composed of partly

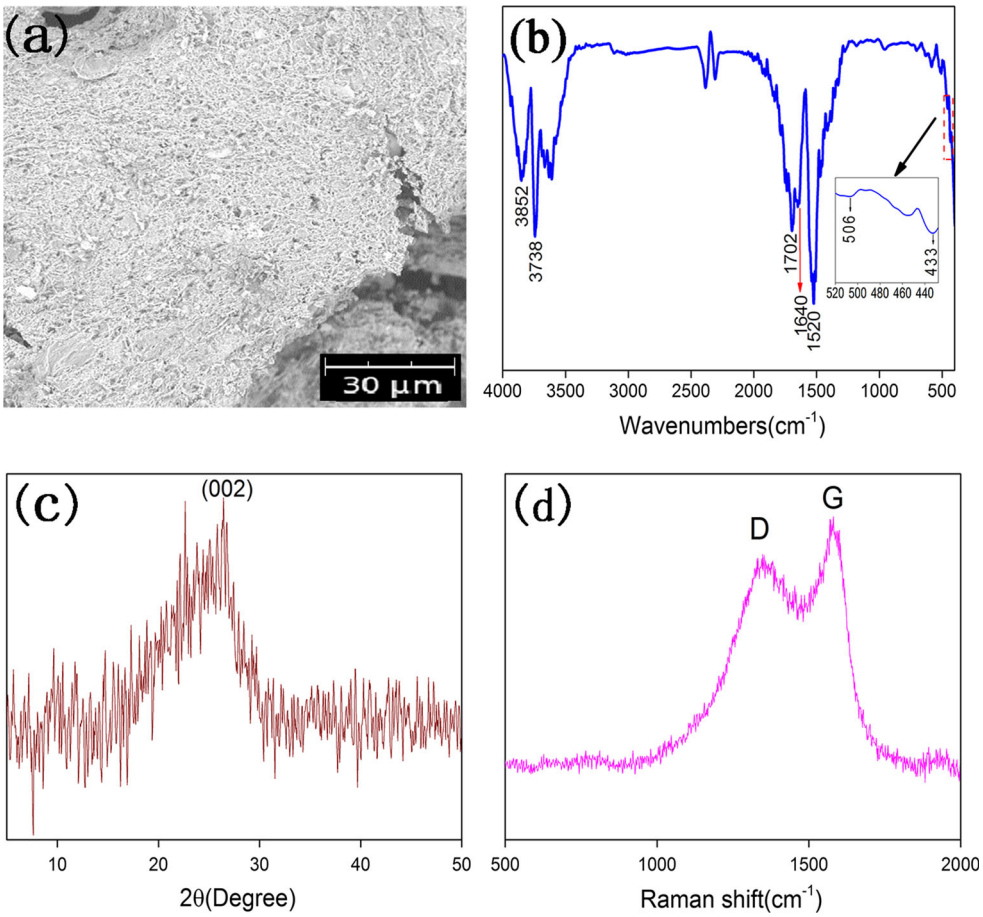

Figure 10 SEM (**a**), FTIR (**b**), XRD (**c**) and Raman (**d**) of the residual char for PLA-2.

graphitized or amorphous carbonaceous materials. The above-mentioned results suggest that the residual char is of partly graphitized structure containing ZnO, aromatic ring structure and other compounds, which effectively limits the heat and mass transfer from the PLA nanocomposites to the heat source.

The intention of using ZIF-8@GO as a flame retardant may be to benefit from chemical and physical barrier mechanisms. With respect to the chemical mechanism, the nitrogen-containing ZIF-8 could give off N_2 and NH_3 that dilutes the ignitable gases during the burning of the composites. The release of water and expansion of GO can also suffocate the flames, which is certified by the reduction in self-extinguishing time of PLA-2 in contrast to that of PLA/ZIF-8 as shown in Fig. 9. On the physical barrier mechanism, the residual char from GO as well as from the partial decomposition of PLA catalyzed by ZIF-8 or the decomposition products of ZIF-8 such as ZnO cuts off the transmission in heat and oxygen, and prevents burning of the nanocomposites [48].

Conclusion

The PLA/ZIF-8@GO nanocomposites with content of 0.05, 0.5 and 2 wt% of ZIF-8@GO were prepared. The ZIF-8@GO particles were well-dispersed in the PLA composites owing to the unique structure of ZIF-8@GO. The crystallinity and crystallization rate of the nanocomposites were increased because of the heterogeneous nucleation effects of ZIF-8@GO. The nanocomposites had improved mechanical properties compared with pure PLA. The LOI of the nanocomposites with 0.5 wt% of ZIF-8@GO was increased to 24.0% compared to 21.0% of pure PLA, and meanwhile, the self-extinguishing time in UL-94 vertical burning test was getting shorter. The ZIF-

8@GO hybrids act as the flame retardants through both chemical and physical barrier mechanisms.

Acknowledgements

This work was supported by Science and Technology Support Program (Social Development) of Jiangsu Province of China (BE 2013714) and a Project Funded by the Priority Academic Program Development of Jiangsu Higher Education Institutions (PAPD).

References

[1] Castroaguirre E, Iñiguezfranco F, Samsudin H, Fang X, Auras R (2016) Poly (lactic acid)—mass production, processing, industrial applications, and end of life. Adv Drug Deliv Rev 107:333–366

[2] Saeidlou S, Huneault MA, Li H, Park CB (2012) Poly (lactic acid) crystallization. Prog Polym Sci 37(12):1657–1677

[3] Bouzouita A, Notta-Cuvier D, Raquez JM, Lauro F, Dubois P (2017) Poly(lactic acid)-based materials for automotive applications. Adv Polym Sci. https://doi.org/10.1007/12_2017_10

[4] Rasal RM, Janorkar AV, Hirt DE (2010) Poly (lactic acid) modifications. Prog Polym Sci 35(3):338–356

[5] Laoutid F, Bonnaud L, Alexandre M, Lopez-Cuesta JM, Dubois P (2009) New prospects in flame retardant polymer materials: from fundamentals to nanocomposites. Mater Sci Eng R 63(3):100–125

[6] Higginbotham AL, Lomeda JR, Morgan AB, Tour JM (2009) Graphite oxide flame-retardant polymer nanocomposites. ACS Appl Mater Interfaces 1(10):2256–2261

[7] Wang HS, Qiu Z (2011) Crystallization behaviors of biodegradable poly(l-lactic acid)/graphene oxide nanocomposites from the amorphous state. Thermochim Acta 526(1):229–236

[8] Zhang CL, Wang TT, Gu XP, Feng LF (2015) Crystallization behavior of functional polypropylene grafted graphene oxide nanocomposite. RSC Adv 5(80):65058–65067

[9] Xu JZ, Chen T, Yang CL, Li ZM, Mao YM, Zeng BQ, Hsiao BS (2010) Isothermal crystallization of poly(l-lactide) induced by graphene nanosheets and carbon nanotubes: a comparative study. Macromolecules 43(11):5000–5008

[10] Kim HW, Yoon JH, Diederichsen KM, Shin JE, Yoo BM, McCloskey BD, Park HB (2017) Exceptionally reinforced polymer nanocomposites via incorporated surface porosity on graphene oxide sheets. Macromol Mater Eng. https://doi.org/10.1002/mame.201700039

[11] Wang X, Song L, Yang H, Xing W, Lu H, Hu Y (2012) Cobalt oxide/graphene composite for highly efficient CO oxidation and its application in reducing the fire hazards of aliphatic polyesters. J Mater Chem 22(8):3426–3431

[12] Cao Y, Feng J, Wu P (2012) Polypropylene-grafted graphene oxide sheets as multifunctional compatibilizers for polyolefin-based polymer blends. J Mater Chem 22(30):14997–15005

[13] Britt D, Tranchemontagne D, Yaghi OM (2008) Metal-organic frameworks with high capacity and selectivity for harmful gases. Proc Natl Acad of Sci USA 105(33):11623–11627

[14] Li S, Yang K, Tan C, Huang X, Huang W, Zhang H (2016) Preparation and applications of novel composites composed of metal-organic frameworks and two-dimensional materials. Chem Commun 47(13):1555–1562

[15] Elangovan D, Yuzay IE, Selke SEM, Auras R (2015) Poly (L-lactic acid) metal organic framework composites: optical, thermal and mechanical properties. Polym Int 61(1):30–37

[16] Petit C, Bandosz TJ (2010) MOF–graphite oxide composites: combining the uniqueness of graphene layers and metal–organic frameworks. Adv Mater 21(46):4753–4757

[17] Petit C, Mendoza B, Bandosz TJ (2010) Hydrogen sulfide adsorption on MOFs and MOF/graphite oxide composites. ChemPhysChem 11(17):3678–3684

[18] Ebrahim AM, Bandosz TJ (2013) Ce (III) doped Zr-based MOFs as excellent NO_2 adsorbents at ambient conditions. Acs Appl Mater Interfaces 5(21):10565–10573

[19] Dasari A, Yu ZZ, Cai GP, Mai YW (2013) Recent developments in the fire retardancy of polymeric materials. Prog Polym Sci 38(9):1357–1387

[20] Poh HL, Šaněk F, Ambrosi A, Zhao G, Sofer Z, Pumera M (2012) Pumera, Graphenes prepared by Staudenmaier, Hofmann and Hummers methods with consequent thermal exfoliation exhibit very different electrochemical properties. Nanoscale 4(11):3515–3522

[21] Chen J, Yao B, Li C, Shi G (2013) An improved hummers method for eco-friendly synthesis of graphene oxide. Carbon 64(11):225–229

[22] Holzwarth U, Gibson N (2011) The Scherrer equation versus the 'Debye–Scherrer equation'. Nat Nanotechnol 6(9):534

[23] Wu D, Cheng Y, Feng S, Yao Z, Zhang M (2013) Crystallization behavior of polylactide/graphene composites. Ind Eng Chem Res 52(20):6731–6739

[24] Nam JY, Ray SS, Okamoto M (2003) Crystallization behavior and morphology of biodegradable polylactide/layered silicate nanocomposite. Macromolecules 36(19):7126–7131

[25] Kumar R, Jayaramulu K, Maji TK, Rao CN (2013) Hybrid nanocomposites of ZIF-8 with graphene oxide exhibiting

tunable morphology, significant CO_2 uptake and other novel properties. Chem Commun 49(43):4947–4949

[26] Bian ZJ, Zhang SP, Zhu XM, Li YK, Liu HL, Hu J (2015) In-situ interfacial growth of zeolitic imidazolate framework (ZIF-8) nanoparticles induced by graphene oxide pickering emulsion. RSC Adv 5(40):31502–31505

[27] Yuan B, Wang B, Hu Y, Mu X, Hong N, Liew KM (2016) Electrical conductive and graphitizable polymer nanofibers grafted on graphene nanosheets: improving electrical conductivity and flame retardancy of polypropylene. Compos Part A-Appl S 84:76–86

[28] Jiang HL, Liu B, Akita T, Haruta M, Sakurai H, Xu Q (2009) Au@ ZIF-8: CO oxidation over gold nanoparticles deposited to metal–organic framework. J Am Chem Soc 131(32):11302–11303

[29] Xiang Q, Yu J, Jaroniec M (2011) Enhanced photocatalytic H_2-production activity of graphene-modified titania nanosheets. Nanoscale 3(9):3670–3678

[30] Fan J, Liu S, Yu J (2012) Enhanced photovoltaic performance of dye-sensitized solar cells based on TiO_2 nanosheets/graphene composite films. J Mater Chem 22(33):17027–17036

[31] Dai X, Cao Y, Shi X, Wang X (2016) Non-isothermal crystallization kinetics, thermal degradation behavior and mechanical properties of poly(lactic acid)/MOF composites prepared by melt-blending methods. RSC Adv 6(75):71461–71471

[32] Zhang J, Jiang L, Zhu L, Jane JL, Mungara P (2006) Morphology and properties of soy protein and polylactide blends. Biomacromolecules 7(5):1551–1561

[33] Kuo SW, Tsai HT (2009) Complementary multiple hydrogen-bonding interactions increase the glass transition temperatures to PMMA copolymer mixtures. Macromolecules 42(13):4701–4711

[34] Arias A, Heuzey MC, Huneault MA (2013) Thermomechanical and crystallization behavior of polylactide-based flax fiber biocomposites. Cellulose 20(1):439–452

[35] Shan GF, Yang W, Tang XG, Yang MB, Xie BH, Fu Q, Mai YW (2010) Multiple melting behaviour of annealed crystalline polymers. Polym Test 29(2):273–280

[36] Gui Z, Lu C, Cheng S (2013) Comparison of the effects of commercial nucleation agents on the crystallization and melting behaviour of polylactide. Polym Test 32(1):15–21

[37] Barrau S, Vanmansart C, Moreau M, Addad A, Stoclet G, Lefebvre JM, Seguela R (2011) Crystallization behavior of carbon nanotube–polylactide nanocomposites. Macromolecules 44(16):6496–6502

[38] Song QL, Nataraj SK, Roussenova MV, Tan JC, Hughes DJ, Li W, Bourgoin P, Alam MA, Cheetham AK, Al-Muhtaseb SA, Sivaniah E (2012) Zeolitic imidazolate framework (ZIF-8) based polymer nanocomposite membranes for gas separation. Energy Environ Sci 5(8):8359–8369

[39] Yao W, Zhao M, Dai Y, Tang J, Xu J (2017) Micro-/mesoporous zinc–manganese oxide/graphene hybrids with high specific surface area: a high-capacity, superior-rate, and ultralong-life anode for lithium storage. Chemelectrochem 4:230–235

[40] Dong S, Tong M, Zhang D, Huang T (2017) The strategy of nitrite and immunoassay human igg biosensors based on Zno@ZIF-8 and ionic liquid composite film. Sens Actuators B Chem 251:650–657

[41] Cui Y, Stojakovic J, Kijima H, Myerson AS (2016) Mechanism of contact-induced heterogeneous nucleation. Cryst Growth Des 16(10):6131–6138

[42] John MJ, Thomas S (2008) Biofibres and biocomposites. Carbohydr Polym 71(3):343–364

[43] Tandon GP, Weng GJ (2010) The effect of aspect ratio of inclusions on the elastic properties of unidirectionally aligned composites. Polym Compos 5(4):327–333

[44] Kathuria A, Abiad MG, Auras R (2013) Toughening of poly(L-lactic acid) with Cu_3BTC_2, metal organic framework crystals. Polymer 54(26):6979–6986

[45] Shi XW, Dai X, Cao Y, Li JW, Huo CA, Wang XL (2017) Degradable Poly (lactic acid)/metal–organic framework nanocomposites exhibiting good mechanical, flame retardant, and dielectric properties for the fabrication of disposable electronics. Ind Eng Chem Res 56(14):3887–3894

[46] Jang JY, Jeong TK, Oh HJ, Youn JR, Song YS (2012) Thermal stability and flammability of coconut fiber reinforced poly (lactic acid) composites. Compos Part B Eng 43(5):434–2438

[47] Feng H, Wang X, Wu D (2013) Fabrication of spirocyclic phosphazene epoxy-based nanocomposites with graphene via exfoliation of graphite platelets and thermal curing for enhancement of mechanical and conductive properties. Ind Eng Chem Res 52(30):10160–10171

[48] Dasari A, Yu ZZ, Mai YW, Cai G, Song H (2009) Roles of graphite oxide, clay and POSS during the combustion of polyamide 6. Polymer 50(6):1577–1587